A&A 411, L261–L268 (2003)
DOI: 10.1051/0004-6361:20031418

Astronomy & Astrophysics

OMC: An Optical Monitoring Camera for INTEGRAL

Instrument description and performance

J. M. Mas-Hesse[1,2], A. Giménez[3], J. L. Culhane[4], C. Jamar[5], B. McBreen[6], J. Torra[7,12], R. Hudec[8], J. Fabregat[9], E. Meurs[10], J. P. Swings[14], M. A. Alcacera[11], A. Balado[11], R. Beiztegui[11], T. Belenguer[11], L. Bradley[4], M. D. Caballero[2], P. Cabo[11], J. M. Defise[5], E. Díaz[11], A. Domingo[2], F. Figueras[7,12], I. Figueroa[11], L. Hanlon[6], F. Hroch[8], V. Hudcova[8], T. García[11], B. Jordan[10], C. Jordi[7,12], P. Kretschmar[13], C. Laviada[11], M. March[11], E. Martín[11], E. Mazy[5], M. Menéndez[11], J. M. Mi[11], E. de Miguel[11], T. Muñoz[11], K. Nolan[6], R. Olmedo[11], J. Y. Plesseria[5], J. Polcar[8], M. Reina[11], E. Renotte[5], P. Rochus[5], A. Sánchez[11], J. C. San Martín[11], A. Smith[4], J. Soldan[8], P. Thomas[4], V. Timón[11], and D. Walton[4]

[1] Centro de Astrobiología (CSIC–INTA), 28850 Torrejón de Ardoz, Spain
[2] Laboratorio de Astrofísica Espacial y Física Fundamental, LAEFF–INTA, PO Box 50727, 28080 Madrid, Spain
[3] Research and Scientific Support Department, ESA, ESTEC, Postbus 299, 2200 AG Noordwijk, The Netherlands
[4] Mullard Space Science Laboratory, University College London, Holmbury St. Mary, Dorking, Surrey, RH5 6NT, UK
[5] Centre Spatial de Liège, Université de Liège, Av. du Pré-Aily, 4031 Angleur, Belgium
[6] Department of Experimental Physics, University College Dublin, Dublin 4, Ireland
[7] Departament d'Astronomia i Meteorologia, Universitat de Barcelona, Av. Diagonal 647, 08028 Barcelona, Spain
[8] Astronomical Institute, Academy of Sciences of the Czech Republic, 251 65 Ondrejov, Czech Republic
[9] Departamento de Astronomía y Astrofísica, Universidad de Valencia, 46100 Burjassot, Valencia, Spain
[10] Dunsink Observatory, Dublin Institute for Advanced Studies, Castleknock, Dublin 15, Ireland
[11] Instituto Nacional de Técnica Aeroespacial–INTA, 28850 Torrejón de Ardoz, Spain
[12] Institut d'Estudis Espacials de Catalunya (IEEC), Gran Capità 2-4, 08034 Barcelona, Spain
[13] INTEGRAL Science Data Centre, Chemin d'Écogia 16, 1290 Versoix, Switzerland
[14] Institut d'Astrophysique et de Geophysique, Université de Liège, Sart Tilman, 4000 Liège, Belgium

Received 15 July 2003 / Accepted 12 September 2003

Abstract. The Optical Monitoring Camera (OMC) will observe the optical emission from the prime targets of the gamma-ray instruments onboard the ESA mission INTEGRAL, with the support of the JEM-X monitor in the X-ray domain. This capability will provide invaluable diagnostic information on the nature and the physics of the sources over a broad wavelength range. Its main scientific objectives are: (1) to monitor the optical emission from the sources observed by the gamma- and X-ray instruments, measuring the time and intensity structure of the optical emission for comparison with variability at high energies, and (2) to provide the brightness and position of the optical counterpart of any gamma- or X-ray transient taking place within its field of view. The OMC is based on a refractive optics with an aperture of 50 mm focused onto a large format CCD (1024×2048 pixels) working in frame transfer mode (1024×1024 pixels imaging area). With a field of view of $5^\circ \times 5^\circ$ it will be able to monitor sources down to magnitude $V = 18$. Typical observations will perform a sequence of different integration times, allowing for photometric uncertainties below 0.1 mag for objects with $V \leq 16$.

Key words. instrumentation: photometers – space vehicles: instruments – techniques: photometric – stars: variables: general

1. Introduction

The International Gamma-Ray Astrophysics Laboratory (INTEGRAL) is dedicated to the fine spectroscopy and imaging of sources in the energy range between 15 keV and 10 MeV. INTEGRAL was launched on Oct. 17, 2002, from Baikonur with a PROTON rocket, into an initial 72-hour orbit with an inclination of 52.5 degrees, a height of perigee of 9000 km and a height of apogee of 154 000 km. More details on the INTEGRAL mission can be found in Winkler et al. (2003) and Jensen et al. (2003). The instrumentation includes a Spectrometer (SPI) and an Imager (IBIS), both using a coded-mask aperture. Two monitors provide additional data in the hard X-ray and optical domains. The Optical Monitoring Camera (OMC) offers the first opportunity to make photometric observations of long duration in the optical band simultaneously with those at X and gamma-rays. OMC has the same field of view (FOV) as the (fully coded) FOV of the X-ray Monitor

Send offprint requests to: J. M. Mas-Hesse,
e-mail: mm@laeff.esa.es

(also using a coded-mask aperture), and is coaligned with the central part of the larger fields of view of the Spectrometer and Imager. Detailed descriptions of the Spectrometer (SPI), Imager (IBIS) and X-Ray Monitor (JEM-X) can be found in this volume. Variability patterns ranging from minutes or hours, up to months and years will be monitored. For bright sources, fast optical monitoring at intervals down to 3 s will be possible.

Multiwavelength observations are particularly important in high-energy astrophysics, where variability is typically rapid, unpredictable, and of large amplitude. In particular, transient events are associated with many kinds of astrophysical phenomena and are of paramount importance in the X and gamma-ray Universe. On the other hand, arranging multifrequency observations that are simultaneous for both ground-based and space-borne instruments is extremely difficult due to weather conditions, scheduling constraints, or technical problems. Therefore, having onboard INTEGRAL an optical monitor like the OMC, adapted to the spatial resolution and field of view of the high-energy instruments, is a powerful additional tool for the understanding of high-energy astrophysical processes.

The main scientific objectives of the OMC are:

- To monitor during extended periods of time the optical emission of all high-energy targets within its field of view, simultaneously with the gamma and X-ray instruments. This will allow the correlation of the optical lightcurves with the variability patterns derived from the hard X-ray and gamma-ray measurements.
- To provide simultaneous and calibrated standard V filter photometry of the high-energy sources. This will allow the comparison of their behaviour with previous or future ground-based optical observations.
- To monitor serendipitously a large number of optically variable sources within its field of view. This will allow the delivery at the end of the mission of a catalogue of thousands of variable sources with a well calibrated optical monitoring, covering periods of minutes to weeks and months.

In addition, as a by-product, the OMC will provide the precise pointing of the instruments with an accuracy of few arcseconds, every 100 s. This information will be available on the ground to improve the image reconstruction of the coded-mask high-energy instruments. The requirement on pointing stability of the spacecraft was around $60''$ (1σ value), although the stability measured during the first months of operations is much better (around $\sigma = 6''$), comparable to the accuracy of the OMC.

OMC has been contributed by the following European institutes:

- Instituto Nacional de Técnica Aeroespacial – Madrid,
- Centre Spatial de Liège,
- Mullard Space Science Laboratory – University College London,
- University College Dublin and Dunsink Observatory Dublin,
- Astronomical Institute Ondrejov,
- University of Barcelona.

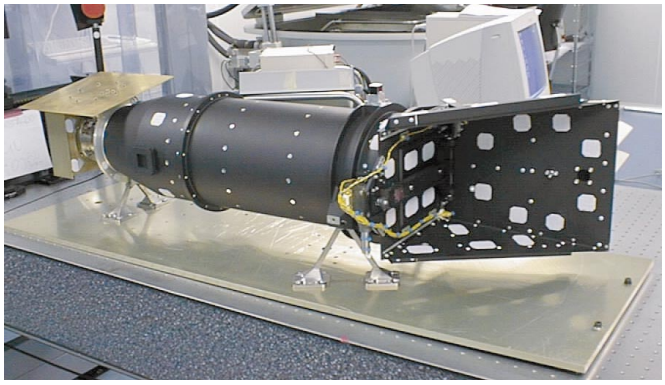

Fig. 1. OMC Camera Unit Flight Model (before installation of the MLI thermal insulation).

In this paper we describe briefly the overall instrument design, scientific performances and operations. Domingo et al. (2003) discuss the OMC Input Catalogue and associated Pointing Software, Walton et al. (2003) present the design of the CCD and associated electronics and finally Mazy et al. (2003) describe the properties of the OMC optics.

2. Camera design

The Optical Montoring Camera (OMC) consists of an optical system focused onto a large format CCD detector working in frame transfer mode (Fig. 1). The layout of the OMC camera unit is shown in Fig. 2. The optics is based on a refractive system with entrance pupil of 50 mm, focal length of 154 mm, and a field of view of $5^\circ \times 5^\circ$. The optical design consists of six radiation-hard glass lenses (F/3) housed in a titanium barrel (see Fig. 3). The filter assembly holds two colored filters (Schott BG39 and GG495) defining a V filter (passband centered at 550 nm) to allow for a straightforward comparison with previous photometric data of the observed targets obtained from ground. An additional BK7G18 glass plate protects the filters from radiation. The optical throughput of the system is slightly higher than 70% at this wavelength, and the CCD quantum efficiency within the V filter passband is around 88%. An LED light source within the optical cavity provides "flat-field" illumination of the CCD for on-board spatial non-uniformities calibration. Both the titanium lens barrel and the focal plane cavity where the CCD is mounted, made of Invar, were coated with black Chromium plating to minimize straylight. The combination of titanium for the lens barrel and Invar for the focal plane cavity allowed to have an almost athermal design, with the system focused over a wide range of temperatures. This allowed to avoid any focusing mechanism.

The stray-light requirements are very stringent and an optical baffle has been designed using ray-tracing simulations to achieve the necessary reduction of scattered sunlight and also the unwanted stray-light coming from non solar sources outside the field of view. A once-only deployable cover protected the optics from contamination during ground preparations (mostly dust particles) and early operations in orbit (outgassing from the spacecraft).

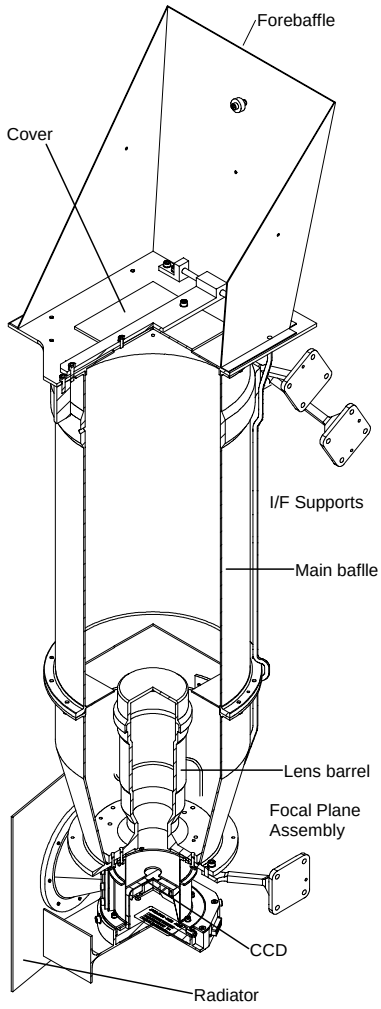

Fig. 2. 3D cut of the OMC Camera unit showing its principal components.

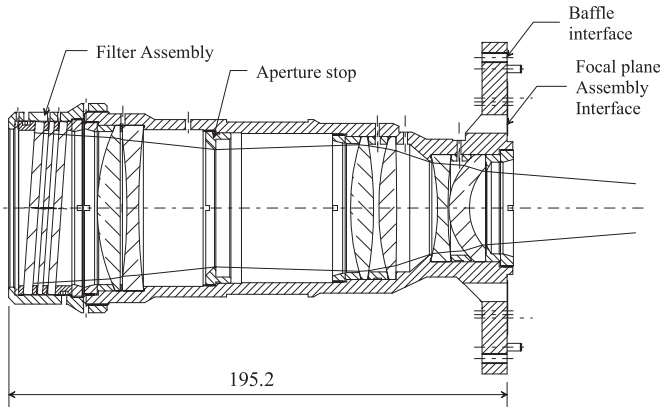

Fig. 3. Layout of the optical system. The length is given in mm.

The CCD (1024 × 2048 pixels) uses one section (1024 × 1024 pixels) for imaging and the other for frame transfer before readout. The frame transfer time of around 0.2 ms avoids the need for a mechanical shutter. The selected chip for the OMC is an EEV CCD 47-20, with an imaging area of 13.3 × 13.3 mm. It required a full qualification program for space applications which was carried out by the OMC consortium. The CCD head

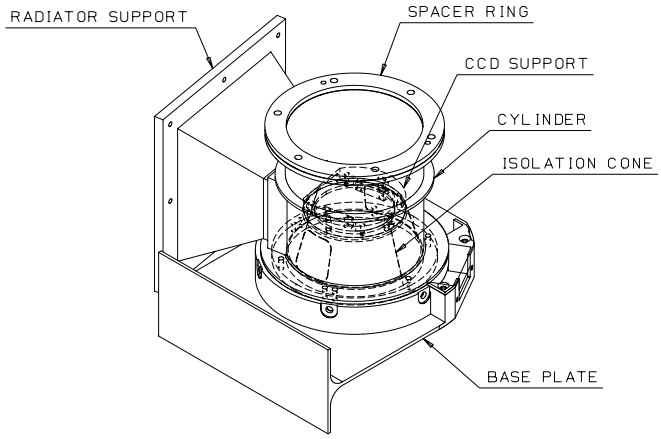

Fig. 4. Layout of the focal plane assembly.

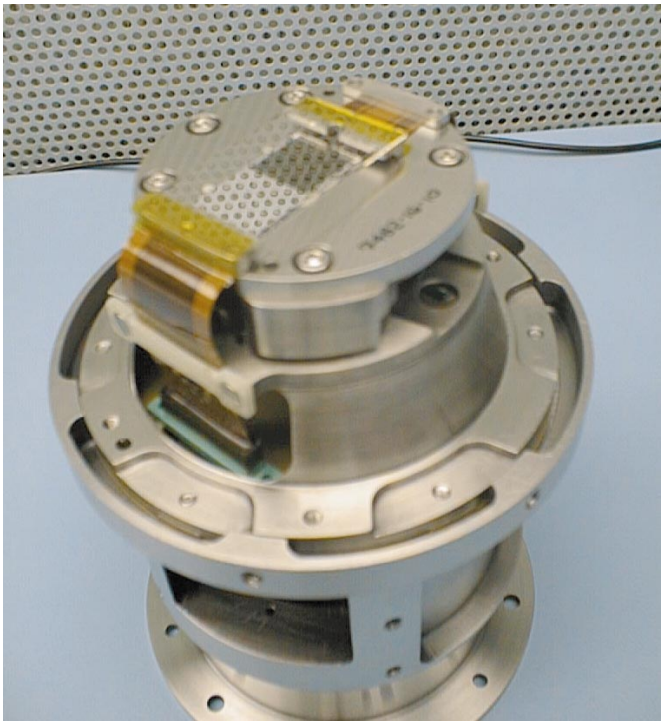

Fig. 5. The Qualification Model EEV 47-20 CCD mounted on its support. Note the reflections of container sides on top of the focal plane surface. The conical structure on which the CCD is mounted is labeled "Isolation cone" in Fig. 4.

is cooled by means of a passive radiator to an operational temperature of around −80 C degrees. We show in Fig. 4 the structure of the Focal Plane Assembly where the CCD is supported, with the identification of the different components, and in Fig. 5 the Qualification Model CCD mounted on its support structure.

The OMC instrument includes also an Electronics Unit, housing the CCD readout electronics, the necessary power conditioning electronics and the corresponding interface with the standard dedicated DPE (Data Processing Electronics) of the spacecraft. The readout mode allows the extraction of only given sections from the CCD instead of the complete frame in order to permit, when needed, fast monitoring of selected stars (while the CCD readout is at a frequency of 300 kHz, the time

Table 1. OMC scientific performances.

Parameter	Value
Field of view	$4.^{\circ}979 \times 4.^{\circ}979$
Aperture	50 mm diameter
Focal length	153.7 mm (f/3.1)
Optical throughput	>70% at 550 nm
Straylight reduction factor (within the unobstructed field of view)	$<10^{-5}$ (for diffuse background)
Point spread function	Gaussian with $FWHM \sim 1.4$ pix (corresponding to $\sim 24.''5$)
Point source location accuracy	$\sim 6''$
CCD pixels	2061×1056 (1024×1024 image area) ($13 \times 13\ \mu m^2$ per pixel)
Image area	13.3×13.3 mm^2
Angular pixel size	$17.''504 \times 17.''504$
CCD Quantum efficiency	88% at 550 nm
Full well capacity	120.000 electrons per pixel
Analogue to digital converter levels	12 bits: ~30 cts/digital level (low gain) ~5 cts/digital level (high gain)
Frame transfer time	~2 ms
Time resolution	≥3 s
Typical integration times	10–100 s
Wavelength range	V filter (centered at 550 nm)
Limit magnitude (10×100 s, 3σ)	17.6 (V)
(50×100 s, 3σ)	18.2 (V)
Sensitivity to variations (10×100 s, 3σ)	$\delta m_V < 0.1$ mag for $V < 16$
Average number of stars per pixel	0.6 (full sky)
($m_V < 19.5$)	2.0 ($b = 0^{\circ}$); <0.1 ($b > 40^{\circ}$)

required to transfer a full image to the DPE memory is around 30 s). The Analogue to Digital Converters (ADC) work with 12 bits, providing a sampling of up to 4096 digital levels.

Several trade-off studies had to be performed during the preliminary design of the OMC. First the field of view was adopted to fit the high-energy instruments, in spite of the loss of photometric accuracy by the increase in the background contribution (diffuse light and source confusion). OMC is thus designed as a monitoring camera adapted to the spatial and photometric resolution required by gamma-ray astronomy, rather than a telescope with high optical performances. The field of view of the OMC complies with the requirement to monitor the main central region of both the Spectrometer and the Imager and is the same as the fully-coded field of view of the other monitor in the X-ray range, so that simultaneous optical and X-ray monitoring of the prime targets can be guaranteed. On the other hand, important science results are expected from simultaneous long-duration V photometry and X-ray data of additional sources in a wide field of $5^{\circ} \times 5^{\circ}$.

The scientific performances and additional parameters of the OMC are finally summarized in Table 1.

Fig. 6. Image of the Large Magellanic Cloud area. The image was obtained by combining a set of 6 individual frames of 10 (2 frames) and 16 s integration time. No processing was made to the image, except removal of the bias level.

3. OMC characteristics and scientific performances

3.1. Optical performance

We show in Fig. 6 one of the first full-field images obtained with the OMC during commissioning of the instrument, corresponding to the Large Magellanic Cloud region. From the analysis of the image it can be seen that the optical properties of the instrument are very homogeneous, both on and off-axis,

Table 2. OMC plate scale as measured on different images.

Image id.	Count	scale vertical ″/pix	scale horizontal ″/pix	sky position RA, Dec (deg)
OMC-first-light.fits	46	17.511	17.498	228, −70
OMC-second-light.fits	46	17.515	17.498	76, −71
multiR6_9012-1.fits	46	17.499	17.506	26, 66
multiR6_9014-1.fit	50	17.506	17.501	26, 66
multiR6_9038-3.fit	67	17.505	17.505	223, 62
multiR6_9039-1.fit	40	17.503	17.506	221,59
multiR6_9052-1.fit	42	17.502	17.506	219, 36

and that no straylight due to reflections within the baffle was reaching the detector.

The astrometric analysis was performed on a set of full field images obtained during the commissioning of the instrument in October–November 2002. All images were processed for the bias, the dark current and the flat-field correction. The resulting images were used as an input to the astrometrical routine of the GAIA software version 2.3–3 (Central Laboratory of the Research Councils), derived from SkyCat version 2.4 (European Southern Observatory).

To process these images, a set of well detected stars was selected by hand on every exposure. A matrix of 5×5 pixels surrounding the central intensity peak for each star was used to get the precise position of the centre of the star. The centre was determined by the weighted arithmetic mean. The centroids, derived in this way, were used as the input data to the astrometric fitting procedure as described by Taff (1981). The pollution of a measured star profile (and consequently of the star centroid) due to the presence of field stars was negligible thanks to the careful selection of star candidates.

The Guide Star Catalogue (GSC) was selected as the reference catalogue for this analysis. The equatorial coordinates of the chosen stars were transformed to rectangular coordinates by the gnomonical projection. The standard astrometric transformation with the scale, the angle of rotation and the coordinate shift was used to determine the parameters of the transformation. The shear and other non-linear terms were excluded.

The results of the fitting procedure together with the basic characteristics of the images are listed in Table 2. The columns in the table give: image identifier, number of coordinate pairs used, derived image scale in vertical and horizontal direction and approximate position of the image centre.

The properties of the OMC Point Spread Function (PSF) can be appreciated in Figs. 7 and 8, where we show the detail of a star image, well centered on a specific pixel. The resulting PSF has a Full Width at Half Maximum $FWHM \approx 1.4$ pix, so that most of the energy is contained within a matrix of 3×3 pixels. The PSF is constant over the whole field of view, with no apparent aberrations (the images are monochromatic, within the Johnson V filter passband). OMC data can therefore be used to derive the pointing of its optical axis with an accuracy close to 5″. This information will be available on the ground and may be used to improve the coded masks image reconstruction on the ground in the future.

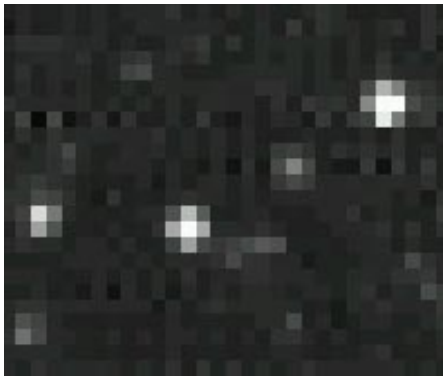

Fig. 7. Image detail, showing the focusing properties of the OMC.

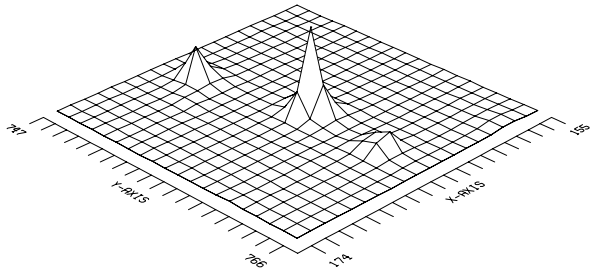

Fig. 8. Surface plot showing the Point Spread Function of the OMC. The axes scale corresponds to physical CCD pixels.

3.2. Photometric performance

The dynamic range covered by the OMC for an integration of 10 s is shown in Fig. 9. It can be seen that a single shot of 10 s allows targets to be observed over a range covering 10 mag. The photometric performance of the instrument is largely limited by its large pixel angular size, which implies significant contributions by faint stars and zodiacal light. In the Galactic Plane, especially, the background associated to faint stars will be significant. At the 3 σ level, and assuming the minimum level of expected background (outside the Galactic Plane), the limiting magnitude of the OMC will be $m(V) = 18.2$ (combining 50 images of 100 s integration each). Note that during a typical pointing of 30 min, the total effective integration time that can be achieved is around 1200 s. For the highest expected background level, i.e., within the Galactic Plane and with largest zodiacal light, the limiting magnitude will be below $m(V) \approx 17.4$ (also for 5000 s effective integrations).

Concerning the bright limit, the full-well capacity of the CCD determines the brightest stars that can be measured

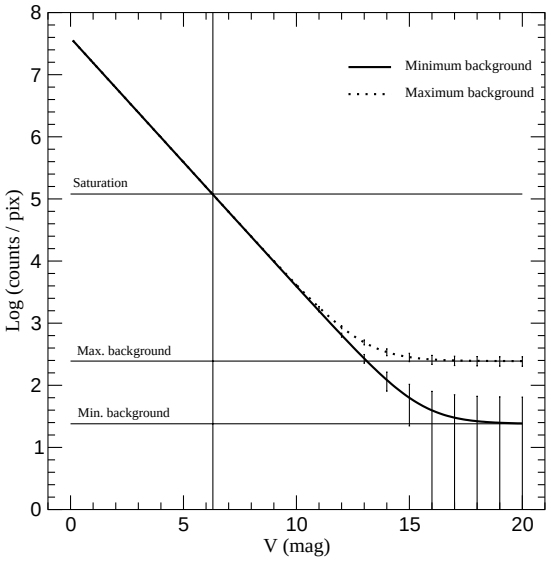

Fig. 9. Number of counts on the central (brightest) pixel as a function of stellar magnitude for an integration time $t_{\rm int}$ = 10 s. The levels corresponding to the maximum and minimum average backgrounds have been indicated, as well as the level at which the CCD saturates. Note that the Analogue to Digital Converters were tuned to sample only the linear response of the CCD, so that the ADC saturates at its maximum level of 4095 DN before the CCD starts to lose linearity.

without pixel saturation for a given integration time (see Fig. 9). OMC is following an observing strategy that combines consecutive integrations of different duration (presently in cycles of 100, 100, 30, 100 and 10 s), thus allowing the effective dynamic range in V magnitude to be extended.

The OMC is able to measure variations in V smaller than 0.1 mag for objects brighter than magnitude 16–17 (depending on background) and smaller than 0.03 mag for objects brighter than magnitude 14, as listed in Table 3. These values have been measured on the set of 10 photometric reference stars per field that are being continuously observed for photometric characterization of the instrument. These reference stars were selected to minimize the effects of nearby overlapping stars. The photometric accuracy achievable on scientific targets will depend strongly on the crowding of the field: stars falling within less than around 50″ of the target source will contaminate the extraction region of 3×3 pixels. Furthermore, a field with many stars will induce a highly structured background, leading also to lower photometric accuracy. Finally, the OMC CCD has suffered the deposition of some contaminants on its surface, especially during the first months of operation. While the effect can be corrected through the flat-fielding process, some residuals at the level of around 1% can still appear when a star is monitored while the spacecraft is dithering from one position to another every 30 min. The rate at which this contamination occurs has been decreasing exponentially since launch. If deemed convenient, the CCD will be baked at 40 C in the future to try to remove the contaminants by using the built-in baking heaters foreseen for this activity.

In any case, very good V photometry can be performed with the OMC for objects of different brightnesses. For the faintest optical sources to be observed by the OMC, at around magnitude $V = 17-18$, photometric detections with sufficient accuracy can be obtained in a similar time to that devoted to the high-energy observations. Several individual photometric points can be produced in the optical band during the gamma-ray measurements and thus light variations as small as 0.5 mag can be detected in those weak objects. In brighter sources, like several of the objects to be observed by INTEGRAL, faster and more accurate photometry can be obtained with the OMC.

Table 3. Photometric accuracy in V magnitudes of the OMC for different V values and various effective integration times. A typical observation totals 300 s of effective integration time.

	V magnitude				
Effective integration time	8	10	12	14	16
10 s	0.007	0.02	0.1	–	–
300 s	–	0.005	0.01	0.04	0.3
900 s	–	0.003	0.006	0.026	0.17

4. Science with the OMC

The observation of high-energy sources in the optical and X-ray domains, simultaneously with spectroscopic and imaging measurements in gamma-rays, will provide the necessary tool for the detailed understanding of the underlying physical processes.

Among the galactic objects to be monitored with the OMC, it is clear that accretion driven binaries with a neutron star or, in particular, a black hole as the compact component, will dominate. Persistent sources hosting a candidate black hole may produce the observed high-energy radiation through the accretion of matter in a deep potential well. Optical light coming from low-mass X-ray binaries is dominated by their luminous accretion disks whose variability can thus be compared with the gamma-ray behaviour. In the case of transient events, X-ray novae or soft X-ray transients will be given most of the attention, though in addition, Be systems showing outbursts in the accretion process on a neutron star will be observed. In the case of binaries with a white dwarf component, the most promising targets for INTEGRAL are classical novae in which a thermonuclear runaway producing a luminous outburst is observed.

Concerning extragalactic research, the OMC will provide photometric data for the multiwavelength analysis of time variability in AGNs. Of particular interest will be the optical variability and periodicity analysis of Blazars, showing fast and unpredictable changes. The comparison of simultaneous measurements in the different energy ranges will indicate the behaviour of different regions of the accretion disk around the central black hole, the relativistic jet, and the reprocessing of radiation. In this context, the observation of optical flares at the time of high energy bursts will also be one of the main objectives in order to determine possible time delays.

Special mention should be made of gamma-ray Bursts. Though the OMC is not designed for the follow-up of GRBs, they will be treated as any other fast high-energy transient by the INTEGRAL alert system. Thus, if one of these events happens in the field of view of the OMC, the instrument will be

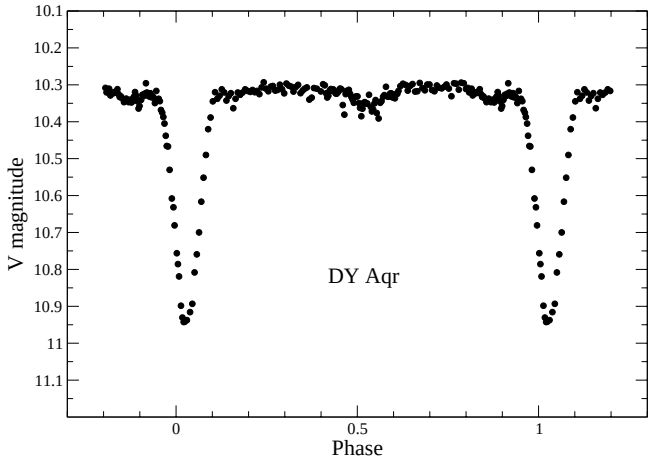

Fig. 10. Light curve of the Algol type eclipsing binary DY Aqr = HD 211705. The derived period is P = 2.1596922 days. The weak secondary eclipse is clearly detected with a depth of only 0.04 mag.

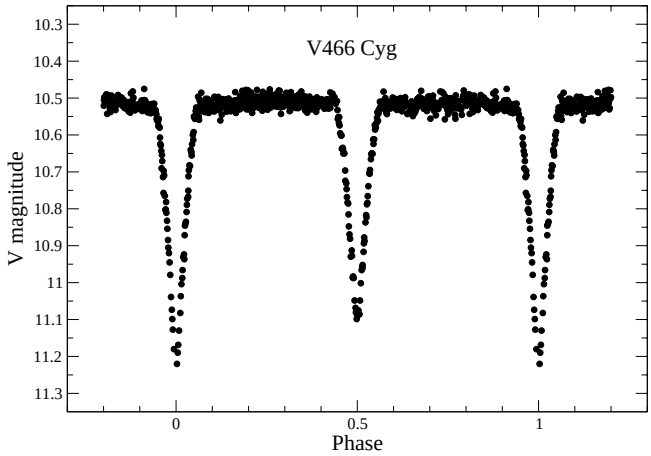

Fig. 11. Light curve of the Algol type eclipsing binary V466 Cyg = HD 331473. The derived period is P = 1.39156705 days. This well detached system is a potential candidate for absolute accurate dimension determination. The depths of the primary and secondary eclipses are found to be 0.7 and 0.6 mag, respectively, in good agreement with previous photographic catalogue data – but not with more recent visual observations.

able to monitor in the optical an area of $30' \times 30'$ around its gamma-ray position within a very short time (few minutes).

In addition to the monitoring of high-energy sources, the operation of INTEGRAL from a high orbit means that particular areas of the sky can be observed virtually continuously for periods of several weeks (with the only interruptions originated by the radiation belts crossing). This will provide a unique photometric capability for the investigation of complex, perhaps multiperiodic, light curves or those objects with periods that cannot be addressed by ground based observers.

At the time of writing this paper more than 20 000 scientific targets have been monitored by the OMC. Out of these, light curves with more than 100 points have been obtained for more than 1300 targets, sampled at intervals of 10 min. We show in Figs. 10–13 some examples of different kinds of eclipsing binaries. Among the eclipsing binaries, four of them are little known since they have been essentially neglected by ground-based photometric observers and only old photographic

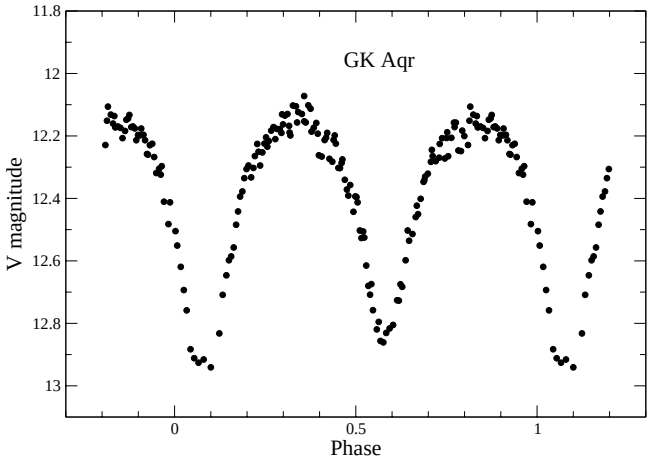

Fig. 12. Light curve of the W UMa type eclipsing binary GK Aqr. Derived period for this system is P = 0.32740976 days.

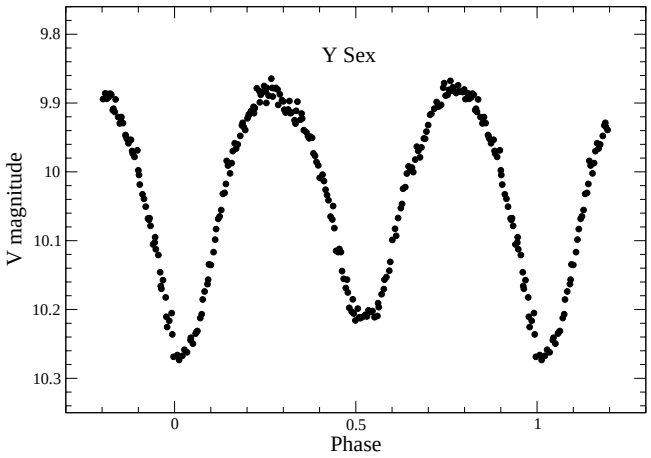

Fig. 13. Light curve of the W UMa type eclipsing binary Y Sex = HD 87079. The period is P = 0.41981485. Note that the difference between the depths of the primary and secondary eclipses is of only 0.06 mag.

light curves are available. For the W UMa type system Y Sex photometric as well as spectroscopic measurements exist and a light curve was obtained with the European satellite Hipparcos. The orbital period variations could be monitored but the new light curve obtained with the OMC clearly supersedes previous data. It can be seen that the sampling of the light curves achieved with OMC is very complete, covering all phases of the orbits.

OMC will be able to produce at the end of its lifetime an extensive catalogue of all kind of variable objects, for many of which simultaneous light curves at hard X-rays and gamma-rays will also be available.

5. OMC operations

In order to optimize the scientific performance of the instrument, the following scientific operating modes have been defined:

a) Calibration mode: The CCD is illuminated by a Light Emitting Diode (LED). The full unbinned frame is read into RAM memory and transferred to Earth.

b) Normal Operation mode: The OMC monitors the sources in its field of view by means of integrations of variable time. Typical values of 30 to 100 s are expected to optimize sensitivity, readout noise, and cosmic rays effects, though shorter values (down to 1 s) are possible to monitor fast variable objects. For the faintest objects, several 100 s exposures are added during data analysis on the ground. The number of integrations that can be added depends on the time during which the spacecraft keeps the same pointing without dithering (typically 30 min). The DPE process the image by first running a fast centering algorithm, based on the location of around 10 bright stars with accurate coordinates in the field. Then, a number of windows (typically of 11×11 pixels) around each object of interest is extracted and transferred to the spacecraft central computer for transmission to ground. Absolute photometric calibration is achieved by comparison with a number of reference standard stars within the field of view of the instrument.

c) Fast Monitoring mode: The normal operations mode does not allow continuous monitoring faster than 10 s due to the speed of the interfaces, the readout electronics and the DPE data handling. Therefore, when fast variability is expected, only the section of the CCD containing the target of interest is read from the CCD and transmitted to the DPE. The best time resolution that can be achieved is around 3 s.

5.1. The OMC input catalogue

Since only a number of windows (typically 100, and in any case less than 228) of 11×11 pixels can be downloaded to Earth, the targets to be monitored have to be pre-selected on ground. For this purpose, an OMC Input Catalogue has been compiled containing:

- most gamma-ray sources,
- most X-ray sources,
- most AGNs within the photometric limits of the OMC,
- most variable stars (including eruptive variable stars, novae and cataclysmics),
- several known additional optical variable objects,
- HIPPARCOS and Tycho reference stars for astrometric and photometric calibration.

During the mission, additional sources of interest are being included in the Catalogue, namely, newly discovered optical counterparts of high-energy sources (in particular sources discovered during the Galactic Plane Survey – see Winkler et al. 2003), regions of special interest for INTEGRAL science, new supernovae and transient sources, or any other Target of Opportunity.

A more complete description of the OMC Input Catalogue can be found in Domingo et al. (2003).

5.2. OMC pipeline processing software

As described above, around 100 CCD windows, each of 11×11 pixels, are downloaded to Earth every 10 to 100 s, without any onboard processing. The data are received at the Integral Science Data Center (Courvoisier et al. 2003), where they are completely processed in an automatic way. The principal steps of this automatic pipeline processing are the following:

- The information in the telemetry packages is converted to CCD pixel values.
- The CCD windows are corrected from bias and dark current. They are then convolved with the corresponding flat-field matrix.
- All CCD windows obtained within periods of around 10 min are combined.
- The photometric value for each source of interest is obtained by applying an extraction mask of 3×3 or 5×5 pixels to the combined images. The local background, as measured on a corona around the extraction mask, is subtracted. The position of the extraction mask is re-centered on the brightest pixel within the 5×5 pixel section. This extraction software can also be run offline modifying the size of the extraction masks, in order to minimize the effects of background stars when needed.
- The photometric values are stored as V magnitudes, thus compiling light curves with a sampling time of around 10 min.

The data products distributed to the observer are the following:

- CCD raw image windows, without any correction.
- Processed and corrected CCD windows (in photoelectrons per pixel).
- Photometric light curve with a sampling time of 10 min (in V magnitude).
- Corresponding flat-field and photometric calibration matrices.

The pipeline processing can be performed off-line in an interactive way, with the capability of modifying some parameters, like the desired sampling or extraction box size (3×3 or 5×5 pixels).

Acknowledgements. We would like to express our gratitude to the many scientists and engineers from the different companies and laboratories that have contributed to the Optical Monitoring Camera. OMC has been partially funded by Spanish MCyT under grants ESP95–0389-C02-02, ESP1997-1803, ESP2001-4531-PE and ESP2002–04124-C03-01. The Czech participation has been supported by the ESA PRODEX Project 14527 and by the Ministry of Education and Youth of the Czech Republic, Project KONTAKT ES036. Additional support was provided under PRODEX Programme in Belgium and Ireland.

References

Courvoisier, T. J.-L., Walter, R., Beckmann, V., et al. 2003, A&A, 411, L53
Domingo, A., Caballero, M. D., Figueras, F., et al. 2003, A&A, 411, L281
Jensen, P. L., Clausen, K., Cassi, C., et al. 2003, A&A, 411, L7
Mazy, E., Defise, J. M., Plesseria, J. Y., et al. 2003, A&A, 411, L269
Taff, L. G. 1981, Computational spherical astronomy (New York: Wiley-Interscience)
Walton, D., Thomas, Ph. D., Culhane, J. L., et al. 2003, A&A, 411, L275
Winkler, C., Courvoisier, T. J.-L., Di Cocco, G., et al. 2003, A&A, 411, L1